

**A 'smart' aptamer-functionalized continuous label-free cell catch-transport-release system**

Journal:	<i>Journal of Materials Chemistry B</i>
Manuscript ID	TB-ART-04-2021-000739.R3
Article Type:	Paper
Date Submitted by the Author:	25-Jun-2021
Complete List of Authors:	Zhang, Bozhen; University of California Los Angeles Wang, Canran; UCLA Du, Yingjie; University of California Los Angeles Paxton, Rebecca; The University of Arizona College of Medicine Phoenix He, Ximin; University of California Los Angeles,

## ARTICLE

# A 'smart' aptamer-functionalized continuous label-free cell catch-transport-release system†

Bozhen Zhang,<sup>‡a</sup> Canran Wang,<sup>‡a</sup> Yingjie Du,<sup>a</sup> Rebecca Paxton<sup>b</sup> and Ximin He<sup>\*a</sup>

Received 00th January 20xx,  
Accepted 00th January 20xx

DOI: 10.1039/x0xx00000x

Label-free cell sorting devices are of great significance for biomedical research and clinical therapeutics. However, current platforms for label-free cell sorting cannot achieve continuity and selectivity simultaneously, resulting in complex steps and limited reliability. Here, an immunoaffinity-based cell catch-transport-release thermo-chemo-mechanical coupling hydrogel (iCatch) device is reported. It contains a temperature-responsive hydrogel that can generate spatial movement synergically with the reversible binding of affinity handle modified. The functionalized hydrogel is embedded inside a biphasic microfluidic platform to enable cell transportation between the flows. The cell sorting capability and biocompatibility of the iCatch device were validated by CCRF-CEM cells as proof-of-concepts and CCRF-CEM-specific aptamers with thermo-responsive affinity as well as hydrogel with temperature-dependent volumes were employed accordingly. A cell catching efficiency of ~40% and a recovery rate of ~70% were achieved. The iCatch device provides a high-throughput (~900 cells·mm<sup>-1</sup>·s<sup>-1</sup>) platform for cell sorting and ultimately valuable for downstream biomedical applications.

## 1. Introduction

Recent advances in microfluidics have further enabled cell separation to take place in simple miniaturized devices for applications such as regenerative medicine,<sup>1, 2</sup> cancer research,<sup>3, 4</sup> and clinical therapeutics<sup>5, 6</sup>, where sorting and isolating target cells from heterogeneous samples are fundamental for subsequent analysis and culture. While there have been a few cell separation approaches used in practice with microfluidic devices, label-free cell sorting has become especially attractive. Label-free cell sorting exploits different cell phenotypical properties and has become a preferential choice because it avoids the high cost of cell labelling and minimizes cell damage.<sup>7-9</sup>

Typically, a physical process-based label-free cell separation relies on internal fluid dynamics forces<sup>10-12</sup> and external forces, such as filtration,<sup>13</sup> centrifugal,<sup>14</sup> acoustophoretic,<sup>15</sup> magnetophoretic,<sup>16</sup> and dielectrophoretic forces,<sup>17, 18</sup> to separate target cells. However, these approaches often require microfluidic devices with dedicated designs and complex fabrications procedures, resulting in limited reconfigurability.<sup>7</sup> Additionally, most of these methods have limited selectivity due to the variance in physical properties among the targeted cells.<sup>19</sup>

In contrast to physical process-based methods, immunoaffinity-based methods rely on chemical interactions between affinity ligands (antibodies or aptamers) and cells to separate cells, which have been reported to have higher selectivity.<sup>20, 21</sup> Based on affinity-

ligand-functionalized materials, these methods include cell affinity chromatograph<sup>22, 23</sup>, pseudo-chromatographic methods<sup>24, 25</sup> and two-phase partitioning<sup>26, 27</sup>. However, these designs require elution or releasing steps<sup>28</sup> (e.g., nuclease,<sup>29, 30</sup> complementary strand,<sup>31, 32</sup> and electrochemical reduction<sup>33</sup>) that are spatially and temporarily separated from the catching step. This discontinuity limits their convenience and efficiency.<sup>34, 35</sup> Currently, few reports have successfully achieved the continuous separation and collection of target cells through an immunoaffinity-based method.

Continuous cell separation has received much attention recently due to lower cost, convenient quality control, and scalability.<sup>36, 37</sup> Notably, compared with intermittent cell separation, continuous separation can release cells in situ following the catching step and allow cells to stay in the same environment with little changes in the surrounding chemical composition, which is crucial for retaining cell functionality. These methods are also promising candidates for rapid, simple, and high-throughput cell separation due to the continuity. Thus, a continuous cell separation device with high selectivity and high throughput is demanded.

'Smart' stimuli-responsive materials can respond to specific signals by changes in mechanical and chemical properties, which makes them promising materials in biomedical applications.<sup>38, 39</sup> By utilizing 'smart' materials synchronized with affinity handles that respond to the same thermal, chemical or mechanical stimuli, we can generate spatial movements and cargo catch-transport-release simultaneously. Thus, the transportation and releasing process are integrated, making the process more streamlined without the complex instrument and time-consuming process. In our previous work, we reported a 'smart' microfluidic system consisting of aptamers and a responsive hydrogel with microscopic fins that achieved chemo-mechanical modulation for continuous biomolecule separation.<sup>40</sup> Similar devices can be employed for

<sup>a</sup> Department of Materials Science and Engineering, University of California, Los Angeles, CA 90095, USA. E-mail: [ximinhe@ucla.edu](mailto:ximinhe@ucla.edu)

<sup>b</sup> University of Arizona College of Medicine - Phoenix, Phoenix, AZ 85004, USA

† Electronic Supplementary Information (ESI) available: Fig. S1-S5 and Video S1-S2. See DOI: 10.1039/x0xx00000x

‡ These authors contributed equally.

controllable continuous inlet separation and spatial cell transportation. However, to expand the capacity of the platform from separating nm-sized proteins to micron-sized cells, the device should be modified for higher binding affinity via enlarging contact surface and optimizing flow rates in the microfluidic device.

Here, we report an immunoaffinity-based cell catch-transport-release thermo-chemo-mechanical coupling hydrogel (iCatch) device that is fabricated with an equipment-free method from a 'smart' hydrogel and affinity handles that are synchronized to respond to temperature changes and realize a sequential and autoregulated target cell sorting and transportation between fluids. The captured cells can be transported and released in situ through the thermally triggered actuation of the 'smart' hydrogel material, resulting in sample-in-answer-out continuous cell separation. The microfluidic system contains three biocompatible components: 1) microfluidic channels that generate two parallel laminar flows for target cell transportation, 2) dynamic affinity handles that can reversibly and responsively catch and release target cells, 3) responsive hydrogel that exerts controllable actuation to transport target cells. In our system, the aptamers, known for high selectivity and scalable production, are employed as the dynamic affinity handles due to their capability to catch and release cells in response to temperature changes reversibly. As the stimuli-responsive hydrogel loaded with aptamers generate thermo-triggered volume changes, it will transport target cells from one stream (upper) to another (lower). The crucial factor of realizing target cell catch-transport-release is that the cell catching and releasing by aptamer are synchronized with the volume changes of hydrogel. To achieve this, the functionalization and denaturation of the aptamers and swelling and contraction of the hydrogels are designed to be both regulated by temperature changes.

To demonstrate the efficiency of our system, we selected the leukemia CCRF-CEM cell line as the model target. Lymphoblastic leukemia is a hemopathy characterized by abnormal white blood cells that occurs in blood and bone marrow.<sup>41, 42</sup> Due to its malignancy, early detection of leukemia cells is required for timely diagnosis and therapy.<sup>43</sup> Accordingly, sgc8c aptamer is selected by cell-SELEX strategy for CCRF-CEM affinity targeting the cell-membrane protein PTK7,<sup>44, 45</sup> and poly(*N*-isopropylacrylamide) (PNIPAAm) hydrogel is selected for its thermo-responsive expansion and contraction.<sup>46</sup> Our 'smart' cell transportation microfluidics realize selective cell binding, controllable transportation between flows, and responsive cell release. In this manner, we developed a controllable thermo-chemo-mechanically modulated microfluidic device for label-free and continuous CCRF-CEM cell sorting with a facile fabrication process.

## 2. Results and discussion

### 2.1 Working principle and design of iCatch device

To achieve immunoaffinity-based cell catch and release, a well-designed responsive material and a matching microfluidic system are required. Our responsive material is a PNIPAAm hydrogel functionalized with sgc8c aptamers (TTT TTT ATC TAA CTG CTG CGC CGC CGG GAA AAT ACT GTA GGG TTA GAT). PNIPAAm is a commonly used thermo-responsive hydrogel that switches from hydrophilic swollen state to hydrophobic shrunk state when the

temperature is raised above its lower critical solution temperature (LCST) of  $\sim 32$  °C.<sup>47-49</sup> The sgc8c aptamer adapts a hairpin structure that is capable of binding to CCRF-CEM cells by recognizing specific membrane proteins (Fig 2C) at temperatures below its melting point ( $T_m = 33.5$  °C).<sup>50</sup> However, when the temperature increases above  $T_m$ , the aptamer will be temporarily denatured and lose its ability to bind to cells. Based on the matching responsiveness and similar critical temperatures of hydrogel and aptamer, these two selected components can respond to temperature changes synergistically (Fig 1A). At RT, the functionalized hydrogel swells, and cells attaches to the nearby aptamers on the hydrogel surface. When the temperature increases to be above their common critical temperatures, the material shrinks and cells are released due to aptamer denaturation. This synergic response makes it possible for the material to transport target cells from one site to another. Thus, in a typical catch-transport-release process, the sample is first pumped into the upper microfluidic channel and the target cells are captured by the aptamers on the swollen hydrogel at room temperature. Then warm buffer is pumped into the lower channel, making the hydrogel contract and release the captured cells into the lower channel. The processed sample can be retrieved from the upper channel and the target cell solution is collected from the lower one.

Unlike our previous work in a pH-responsive protein-catching hydrogel,<sup>40</sup> the iCatch system is designed to catch cells rather than proteins, therefore requiring higher binding affinity due to larger cargo volumes. To address this challenge, we fabricated the hydrogel as a non-structured thin film directly functionalized with aptamers instead of using aptamer-carrying epoxy microfins mounted on the hydrogel. This design endows our 'smart' hydrogel with increased contact area for cells as well as continuous interaction with multiple proteins on the cell membrane. Such a simplified design is more feasible for catching cells than proteins because cells are large enough to avoid being absorbed into the pores of a non-structured hydrogel. Additionally, it accelerates the response of the material due to the removal of the non-responsive epoxy. Another difference between the iCatch system and the protein-catching system is that a thermal stimulus is used instead of pH stimulus. This stimulus is more advantageous for remote delivery and applicable to more cargos (e.g., cells) without changing their chemical environment.

For the microfluidic system, we used a straightforward two-channel design. The design is illustrated in Fig 1C. Two channels with distinct inlets and outlets are placed above the hydrogel on glass substrate. The mixture solution is pumped into the upper channel, while the sorted CCRF-CEM cells flow out from the lower channel. The channels are simply formed from laser-cut double-sided tapes, which makes the system highly cost-efficient and reconfigurable. Laminar flows in the channels are guaranteed by controlling the flow rates. In a typical cell sorting process (Fig 1B), we begin with the swollen hydrogel with its top surface in the upper channel at room temperature, catching the targeted cells flowing in the mixture solution. Warm buffer is then pumped into the lower channel, heating the hydrogel to a temperature above its critical temperature. The hydrogel shrinks so that its top surface is immersed in the lower channel. The aptamers are denatured, and the cells are released into the channel due to the warm buffer. The aptamers do not contact the warm buffer in the lower channel and denature before the hydrogel shrinks, which prevents captured cells from being released to the upper channel (detailed discussion on the responding sequence of aptamer and hydrogel can be found in **Note S1**).

The sorted cells and residue solution are collected separately from two outlets following a Y-shaped junction.

In cell catching of the microfluidic system, the mild shear force provided by the microfluid also assists with the cell attachment on the hydrogel, which resembles the cell attachment of leukocytes on vascular endothelial cells during leukocyte recruitment to inflamed tissues.<sup>51,52</sup> In this process, the shear forces result in the rolling and deformation of recruited cells, which enhance the contact area with the targeted surface and the probability of forming multiple bindings between cells and aptamers. All of these factors lead to sufficient interaction between cells and the functionalized hydrogel surface. Our previous simulation study on the catching and releasing behaviour of aptamers immobilized on hydrogels in fluid further confirms our design.<sup>53</sup>

To determine whether the aptamers were successfully attached to the hydrogels, UV absorption experiments were conducted. The UV absorption spectra of pure PNIPAAm and hydrogel synthesized with different concentration of acrydite-functionalized aptamers are shown in Fig 2D. The features at 260 nm, which can be assigned to DNA only present in the spectra of functionalized hydrogels, which confirms that the functionalization was successful.<sup>54</sup>

The UV absorption results indicates the chemical composition in the bulk material, while the material surface is more crucial for cell-material interactions. Therefore, XPS was further conducted to acquire information on the surface elemental composition of the material. The XPS results of functionalized hydrogel and pure PNIPAAm are shown in Fig 2E and Fig S2. Both spectra contain C 1s, N 1s, and O 1s signals, while the phosphorous signal from the phosphate group in DNA was only detected in functionalized hydrogel (Fig 2E and S1). This confirms that there were exposed aptamers at the surface of the aptamer-functionalized material.

To characterize the geographic response of the hydrogel to thermal stimuli, we assessed its temperature-induced volume change (Fig S2). Upon a sudden heating up (from room temperature to around 32°C), the thickness of the gel decreased rapidly, while it slowly recovered to the original state when temperature gradually fell (Video S1). The relationship between hydrogel thickness and the temperature is demonstrated in Fig 2F, showing a maximum shrinkage of 37% at a rate of 12  $\mu\text{m}/^\circ\text{C}$ . This fast response shows the high sensitivity of the hydrogel part of the device.

## 2.2 Evaluation of iCatch capability of selective cell catch-transport-release

For affinity-based microfluidic cell sorting, non-specific interactions with the device components should be avoided. PNIPAAm surface is known for cell adhesion after co-culturing for a long term.<sup>54,55</sup> We anticipated that the porous hydrogel aside the aptamers would not trap cells in minutes during the cell separation. Indeed, when we incubated cells on the surface of PNIPAAm without and with sgc8c aptamer modification for 10 mins, CCRF-CEM cell attachment was only observed in the latter group (Fig. 3A). Compared with 20 $\pm$ 12 cells/ $\text{mm}^2$  for bare PNIPAAm, the cell density on aptamer-modified hydrogel could achieve 905 $\pm$ 273 cells/ $\text{mm}^2$ , indicating the aptamer-functionalized hydrogel's capacity for high-throughput cell catching (Fig. 3B). Apart from preventing non-specific interaction between the cells and the hydrogel, realizing certain selectivity among different cell species is required to achieve cell sorting. We

confirmed the selectivity of our system by using RAMOS cells that have no affinity with sgc8c aptamers as the control group. As it was shown in Fig. 3A and 3B, after incubation, the captured Ramos cells were at a density of 98 $\pm$ 21 cells/ $\text{mm}^2$ . The captured cell density for CCRF-CEM cells was 10-time higher than that for Ramos cells, demonstrating the cell-specific affinity and selectivity of our system.

We verified that the selectivity of cell catching was attributed to sgc8c aptamers immobilized on the hydrogel by introducing scrambled aptamers with acrydite linkers for immobilization and sgc8c aptamers without acrydite linkers to the PNIPAAm hydrogel. The cell affinities of each group were defined as the density of cells remaining after incubating and washing. Our experimental group, utilizing sgc8c aptamer with acrydite linker, exerted significantly higher cell density over the group utilizing scrambled aptamers (60 $\pm$ 50 cells/ $\text{mm}^2$ ) and the group without acrydite linkers (20 $\pm$ 13 cells/ $\text{mm}^2$ ) (Fig. S3). Collectively, these results demonstrated the importance of covalent aptamer attachment and cell-specific designs in catching cells with high selectivity and efficiency.

To evaluate the performance of the aptamers in thermo-responsive cell 'catch-transport-release', we first conducted experiments to assess the cell density changes on the aptamer-functionalized hydrogel at various time points (1, 5, and 10 mins) when the temperature increased to 45°C from room temperature (RT). After one-min incubation and 30 s wash at 45°C, cell release was quantified. It was evident that the cell release was triggered at an increased temperature (Fig. 3C). The quantification in Fig. 3D indicated that the cell density after releasing was 207 $\pm$ 65 cells/ $\text{mm}^2$  and thus recovery rate of our system reached 77.2%. To confirm that the cell release was not caused by the mechanical force generated by the flow, we washed the aptamer-hydrogel at room temperature (RT) first and subsequently at 45°C. It was observed that most cells were washed away at elevated temperatures (Fig.S4), further confirming the thermo-responsive cell releasing capability. Additionally, the catching of cells in the flow and remaining of cells after washing at RT both indicated that the binding affinity between aptamer and cells could be maintained in spite of the shear force generated from the flow (Fig. S4). We also observed that only 25 $\pm$ 17 and 18 $\pm$ 9 cells/ $\text{mm}^2$  remained attached to the pure PNIPAAm hydrogel at RT and 45°C, respectively (Fig. S5), suggesting limited non-specific interaction with hydrogel in the whole process. Notably, one cycle of the catch-transport-release process was finished in 12 mins. The ability for rapid and high-throughput cell sorting in our simply controlled device makes it suitable for dealing with large samples.

Maintaining biocompatibility during cell separation is also required for preventing cell damage before further analytical applications. It is essential to test whether the short-term temperature elevation and aptamer affinity influence cell viability. We characterized the cell conditions by conducting the Live & Dead staining assay. It was observed that after flowing through the channel, 86 $\pm$ 4% of total cells were alive in the buffer. Particularly, 78 $\pm$ 6% of cells remained alive after one "catch-transport-release" cycle, suggesting excellent biocompatibility of our system (Fig. 3E). Taken together, these results proved the capability of our aptamer-hydrogel system in selective cell 'catch-transport-release' in responsive to temperature change with good compatibility. It is worthy to note that thermo-responsive aptamers could realize cell catching at RT and release at 45°C, synchronizing

with the swelling and contraction of the hydrogel, respectively.

We applied the aptamer-hydrogel system to a microfluidic chip to investigate the cell sorting capability of our whole device by firstly pumping cells at the concentration of  $5 \times 10^6/\text{mL}$  in the device. Non-specific interaction is one common issue that should be dealt with in cell sorting devices. As it was shown in Fig. 4A, this aspect was not presented in the control group, where the hydrogel inside the microfluidic device was not modified with aptamers, suggesting the affinity is mediated by aptamers. The quantitative characterization further confirmed the specific interaction between cells and iCatch device. Compared with the iCatch device, where the cell density reached 863 cells/ $\text{mm}^2$ , the non-aptamer modified group only caught cells at a density of 72 cells/ $\text{mm}^2$ , which is consistent with our results in hydrogel material with and without aptamer (Fig. 4B).

Then the efficacy of the thermo-chemo-mechanical modulated cell separation device was assessed. As it was shown in Fig. 4C and Video S2, when warm buffer was pumped to the device, the hydrogel contracted and generated spatial movement. At the same time, the captured CCRF-CEM cells were released from hydrogel in few mins, demonstrating the thermo-chemo-mechanically modulated cell separation with high efficiency. After releasing, the density of cells remaining in the device was decreased to 272 cells/ $\text{mm}^2$  from 915 cells/ $\text{mm}^2$  with 70% recovery rate approximately (Fig. 4D). Accordingly, the throughput of iCatch device could be calculated as 888 cells· $\text{mm}^{-1}$ · $\text{s}^{-1}$ . Additionally, the throughput of cell sorting could be further optimized by increasing the hydrogel surface area and aptamer modification density. We also tested the limitation of detection (LOD) of iCatch device. It was calculated from Figure 4B that the 3% of the cells could be caught in the device without aptamer, which was set as the threshold of detection. A series of experiments were then conducted with cell concentration range from 10 to  $5 \times 10$  cells/ $\text{mL}$ . It was observed that the LOD of iCatch device could reach 100 cells/ $\text{mm}^2$ . The LOD correlates with many previous reports on sgc8 aptamer-mediated CCRF-CEM cell detection, indicating that our design maintained the selectivity and sensitivity of aptamer as the key catching agent.<sup>56,57</sup>

In summary, we have developed a miniature iCatch device for cell sorting integrated with thermo-responsive aptamers catch-release and PNIPAAm hydrogel swelling and contraction to realize target cell spatial movement in a synergistic way. It is observed that iCatch device yields high-throughput (888 cells· $\text{mm}^{-1}$ · $\text{s}^{-1}$ ), efficient (39.4% in 15 s) and effective (>70% recovery rate) on CCRF-CEM cell sorting.<sup>9, 58</sup> Due to the continuous manner of the cell catch-transport-release process, the cell solution which has been processed once could be pumped back to the microfluidic device and be processed repeatedly. The cycling enabled by the continuity could further increase the catching efficiency. Besides, the efficiency could be improved by altering the concentration of aptamers and the cell solution. For recovery rate, it can be further enhanced by tuning the response rate, releasing time and flow rate of warm buffer. The reversibly responsive components, aptamer and PNIPAAm hydrogel, in the iCatch device work synergistically, enabling the continuous and cyclable label-free cell sorting and guaranteeing the high selectivity at the same time. This synergism also integrates the transport and release processes, which shortens the operation time. Also, the microfluidic design endows the device with high throughput. The facile fabrication of iCatch device can reduce the

cost for scaling up as well. These advantages address many challenges in cell sorting, particularly when dealing with large amounts of samples. Compared to high-throughput continuous physical process-based methods<sup>59,60</sup>, such as inertial based ones, the selectivity of our method is higher owing to the immunoaffinity-based mechanism. Compared to other stimuli-responsive continuous immunoaffinity-based methods, such as electric-field-based ones<sup>61,62</sup>, iCatch has higher throughput and its fabrication is simple. Though its one-cycle catching efficiency is limited, the separation rate could be enhanced by increasing the cycling number. Additionally, compared with triggers such as electric fields and pH changes, regulating responsive materials by temperature is preferred due to less alternation in cell properties such as membrane electric potential.<sup>7, 63</sup> We proved that the isolated cells from iCatch device can maintain their viability, which is essential for downstream research and clinical applications.

Although we tailored iCatch for CCRF-CEM cell sorting as a proof-of-concept, realizing a high catching efficacy ( $\sim 900$  cells/ $\text{mm}^2$ ), it is easy to design aptamer sequences by cell-SELEX strategies and optimize fabrication parameters (aptamer concentration and hydrogel volume) to serve the demands of sorting various cells and reaching even higher efficiency. For instance, in future applications, iCatch can be adjusted to extract T cells from peripheral blood mononuclear cells (PBMC) for immunotherapy preparation.<sup>64</sup> It can also be integrated into other sample-in-answer-out microfluidic platforms as an independent module. Additionally, with the advancement in SELEX strategies, the iCatch device applications could be expanded. Compared to antibodies, aptamer-cell interactions dependent on cell surface properties rather than specific protein markers. It enables distinguishment of even a small subset of cells for disease early detection.<sup>65, 66</sup> With the merits of ease of use, high-throughput, and scalability, we conclude that our iCatch device provides a powerful cell sorting platform that will benefit broad applications ranging from biomedical research to clinical diagnostics and therapeutics.

As a proof-of-concept study, thermal-regulated continuous and high-throughput cell separation has been achieved in this work.

To further understand the microscopic process of catch-transport-release, more computational simulation could be useful. To promote the practical applications of this system, body fluid with more complicated components could be used and microfluidic devices in series for sequential separation of various cells could be fabricated in further research. Due to the separation of catching and releasing sites, the target cells are able to be collected while still remaining in an environment similar to the original mixture. That makes it possible to conduct continuous rounds of cell separation of one mixture to further increase the separation efficiency and maintain the health and functionality of the cells. In the future, the iCatch devices can also be connected in series to separate different cells continuously from a practical mixture of interest.

## 3. Experimental

### 3.1 Chemicals

3-(trimethoxysilyl)propyl methacrylate (Sigma M6514), *N*-isopropyl acrylamide (NIPAAm), *N,N'*-methylenebisacrylamide (BIS), *N,N,N',N'*-tetramethylethylenediamine (TEMED) and Ammonium persulfate (APS) were purchased from Sigma-Aldrich. Sgc8c Aptamer and scrambled aptamer were purchased from Integrated DNA Technologies. Polydimethylsiloxane (PDMS)

(Dow-Sylgard 184) was purchased from Ellsworth.

### 3.2 Surface modification of glass

We used glass slides as the substrate for synthesizing the hydrogel. The glass substrates were modified by silanization, which was inspired by a previous reported method.<sup>67</sup> Glass cover slides were cleaned by ultrasonication for 30 min in a soap solution (ALconox) and acetone. Then the slides were washed with ultra-pure water and air dried. Afterwards, they were immersed in a silanization solution which was prepared by diluting 1 mL of 3-(trimethoxysilyl)propyl methacrylate in 200 mL ethanol. Prior to immersion, 6 mL of an acetic acid solution (1: 10 glacial acetic acid: water) was added to the solution. The glass slides were then incubated for 1 h, until the reaction was terminated by a wash with ethanol followed by water.

### 3.3 Synthesis of aptamer-functionalized hydrogel

A precursor solution was prepared by dissolving 70.0 mg NIPAAm, 1.5 mg BIS and 5.0  $\mu$ L TEMED in 600  $\mu$ L demineralized water and purging the solution for 30 min in a water/ice bath. Afterwards, 400  $\mu$ L of 500  $\mu$ M aptamer (or 200  $\mu$ L of 500  $\mu$ M aptamer and 200  $\mu$ L demineralized water for hydrogel with low aptamer concentration for characterization) and 13.3  $\mu$ L of 0.5 M APS were added to initiate the reaction. The solution was mixed and transferred to a petri dish in 5  $\mu$ L aliquots. Silanized glass slides and cover slides serving as spacers were put on top of the solution droplets. The solution was then left to cure for 2 hours at room temperature, and aptamer-functionalized gel attached to glass slides were obtained. After the glass slides were peeled off, the hydrogels were washed for two days in 1X TBE (Tris/Borate/EDTA, pH = 8) to remove unreacted components.

### 3.4 Microfluidic device fabrication

The microfluidic device was composed of 4 layers: the bottom layer of responsive hydrogel on glass, the top layer of flat PDMS, and two layers of double-sided adhesive tapes with laser cut pattern in between. The rectangular hydrogel (0.5 mm  $\times$  8 mm) with aptamer was synthesized by using the method mentioned above, on top of which the patterned adhesive tapes were placed. There were rectangular channels with the same size of the hydrogel on both tapes. Aside them, there were distinct inlet and outlet holes, allowing 2 independent paths for fluids. To collect two separate solutions from these paths, the microfluidic channel was designed to branch into two outlets with a Y-shaped junction, diverting the fluids to distinct collection outlets. Subsequently, the channels and holes were capped with a PDMS sheet integrated with PDMS tubing, allowing inlet of fluid from syringe pumps and outlet to collection devices. The calibrated flow rates of the pumps were used to define and maintain the two layers of fluids laminar flows.

### 3.5 Chemical characterization

UV absorption spectroscopy of the thermo-responsive materials with 2 different aptamer concentration was obtained with a plate reader (Multiskan SkyHigh, Thermo-fisher, USA). Pure PNIPAAm was used as reference. X-ray photoelectron spectroscopy of the hydrogel was obtained with an XPS (Thermo K-alpha XPS, Thermo-fisher, USA, beam size 400  $\mu$ m) after it was dried.

### 3.6 Thermo-responsive swelling test

To investigate the thermo-responsivity of the functionalized PNIPAAm hydrogel, the hydrogel swelling in different temperatures was monitored with confocal microscopy (SP5 TCS confocal microscope, Leica, Germany, 10x objective). Fluorescent

spheres with a diameter of 1  $\mu$ m were applied to the sample to ease the visualization of the gel. The sample was immersed into hot water and the temperature was allowed to equilibrate to room temperature, while the temperature was measured with a thermal couple simultaneously. In this process, the thickness of the gel was monitored by capturing z-stacks of a specific part of the gel every 60 s. A temperature change cycle approximately lasted 10 min. The experiment was also repeated by adding hot water to swollen hydrogel. Fluorescent images were collected with an excitation wavelength of 488 nm and an emission range of 500-570 nm. Each z-stack contained 270 slices with 1  $\mu$ m spacing and was acquired with a Leica DMI#3000.

### 3.7 Cell culture and staining

CCRF-CEM cells (CCL-119, ATCC, USA) and Ramos cells (CRL-1596, ATCC, USA) were grown in RPMI 1640 medium supplemented with 10% fetal bovine serum and 1.2% Penn Strep antibiotic. Cell solutions were stored at 37°C in a humidified incubator containing 5% CO<sub>2</sub>. Prior to the cell experiments, cells were suspended to obtain a cell concentration of 5 $\times$ 10<sup>6</sup> cells/mL. Here, a cell binding buffer was employed since normal cell media contain nucleases that are potentially harmful to the aptamers. For cell visualization, samples were labeled with Vybrant dye (DiI, Invitrogen, USA) according to protocol provided by the manufacturer.

### 3.8 Cell catch-and release experiment of hydrogels

For cell catch experiments, samples were incubated with the CCRF-CEM cell solution (5 $\times$ 10<sup>6</sup> cells/mL) at room temperature for varying amount of time (1, 5 and 10 mins). Afterwards, unbound cells were removed by placing 50  $\mu$ L of the cell binding buffer on top of each hydrogel and shaking the sample at 90 rpm for 30 s on an orbital shaker. The remaining attached cells were imaged with an inverted fluorescent microscope (Olympus IX71, Munday Scientific, USA) and counted manually. For cell release, samples were incubated at 45 °C for 1 min in the oven. Subsequently, the cell catch was converted to cell release by adding 50  $\mu$ L cell binding buffer with a temperature of 45 °C. The detached cells were gently removed by shaking the sample at 90 rpm for 30 s and the remaining attached cells were imaged using the inverted microscope.

### 3.9 Live/dead staining

Staining for cell viability assessment was performed by LIVE/DEAD Viability/Cytotoxicity kit (Invitrogen, USA) as protocols provided by the manufacturer. After incubating 30 min, samples were washed by DPBS gently and detected by fluorescent microscope at the wavelength of 488 nm and 544 nm.

### 3.10 Cell catch-and-release experiment on iCatch device

At RT, 100  $\mu$ L of cell solution (2% (vol/vol) fetal calf serum in PBS, 5  $\mu$ L/min) was flowed into the top layer at the same times as 100  $\mu$ L of buffer (20  $\mu$ L/min) was flowed into the bottom layer. The cell solution eluted from the top layer was collected and reflowed into the channel for 10 cycles, until 45°C buffer (20  $\mu$ L/min) was flowed into the bottom layer to collect the released cells that were captured by the hydrogel surface. The catching efficiency and the cell recovery rate in iCatch device were calculated as follows:

$$\text{Efficiency\%} = [\text{Total number of cells caught on the device} / (\text{Flow rate of cells} * \text{Cell solution flowing time})] * 100\%$$

$$\text{Recovery rate\%} = [1 - (\text{Total number of cells remaining on the device after releasing}) / (\text{Total number of cells on the device before releasing})] * 100\%$$

$$\text{Throughput} = \text{two-dimensional density of captured cells} \times$$

velocity (Derivation of this expression can be found in **Note S2**).

### 3.11 Video Imaging and cell quantification

To quantify the cell “catch-transport-release” properties of iCatch, the whole process was imaged with movies taken by camera (Olympus IX71, Munday Scientific, USA). Cells were quantified by ImageJ program (National Institute of Health, USA)

### Conflicts of interest

There are no conflicts to declare.

### Acknowledgements

The work was supported by NSF CAREER award 1724526.

### References

1. P. Zhang and A. R. Abate, *Adv. Mater.*, 2020, **32**, e2005346.
2. R. N. Judson, M. Low, C. Eisner and F. M. Rossi, *Methods Mol. Biol.*, 2017, **1668**, 93-103.
3. S. C. Hur, J. Che and D. Di Carlo, *Methods Mol. Biol.*, 2017, **1634**, 65-79.
4. N. Sun, X. Li, Z. Wang, Y. Li and R. Pei, *Biosens. Bioelectron.*, 2018, **102**, 157-163.
5. M. Labib, Z. Wang, S. U. Ahmed, R. M. Mohamadi, B. Duong, B. Green, E. H. Sargent and S. O. Kelley, *Nat. Biomed. Eng.*, 2021, **5**, 41-52.
6. T. N. G. Adams, A. Y. L. Jiang, N. S. Mendoza, C. C. Ro, D. H. Lee, A. P. Lee and L. A. Flanagan, *Biosens. Bioelectron.*, 2020, **152**, 111982.
7. R. Nasiri, A. Shamloo, S. Ahadian, L. Amirifar, J. Akbari, M. J. Goudie, K. Lee, N. Ashammakhi, M. R. Dokmeci, D. Di Carlo and A. Khademhosseini, *Small*, 2020, **16**, e2000171.
8. S. Zhang, Y. Chen, H. Liu, Z. Wang, H. Ling, C. Wang, J. Ni, B. Çelebi-Saltik, X. Wang, X. Meng, H.-J. Kim, A. Baidya, S. Ahadian, N. Ashammakhi, M. R. Dokmeci, J. Travas-Sejdic and A. Khademhosseini, *Adv. Mater.*, 2020, **32**, 1904752.
9. H. Tavassoli, P. Rorimpandey, Y. C. Kang, M. Carnell, C. Brownlee, J. E. Pimanda, P. P. Y. Chan and V. Chandrakanthan, *Small*, 2021, **17**, e2006176.
10. Z. Liu, R. Chen, Y. Li, J. Liu, P. Wang, X. Xia and L. Qin, *Adv. Biosyst.*, 2018, **2**, 1800200.
11. X. Zhang, Z. Zhu, N. Xiang, F. Long and Z. Ni, *Anal. Chem.*, 2018, **90**, 4212-4220.
12. J. Feng, J. Mo, A. Zhang, D. Liu, L. Zhou, T. Hang, C. Yang, Q. Wu, D. Xia, R. Wen, J. Yang, Y. Feng, Y. Huang, N. Hu, G. He and X. Xie, *Nanoscale*, 2020, **12**, 5103-5113.
13. T.-C. Sung, W.-L. Huang, L.-K. Ban, H. H.-C. Lee, J.-H. Wang, H.-Y. Su, S. H. Jen, Y.-H. Chang, J.-M. Yang, A. Higuchi and Q. Ye, *J. Mater. Chem. B*, 2020, **8**, 10577-10585.
14. L. Yin, Z. Yang, Y. Wu, V. Denslin, C. C. Yu, C. A. Tee, C. T. Lim, J. Han and E. H. Lee, *Biomaterials*, 2020, **240**, 119881.
15. P. Li, Z. Mao, Z. Peng, L. Zhou, Y. Chen, P.-H. Huang, C. I. Truica, J. J. Drabick, W. S. El-Deiry, M. Dao, S. Suresh and T. J. Huang, *Proc. Natl. Acad. Sci. U. S. A.*, 2015, **112**, 4970.
16. W. Zhao, T. Zhu, R. Cheng, Y. Liu, J. He, H. Qiu, L. Wang, T. Nagy, T. D. Querec, E. R. Unger and L. Mao, *Adv. Funct. Mater.*, 2016, **26**, 3990-3998.
17. N. Sobahi and A. Han, *Biosens. Bioelectron.*, 2020, **166**, 112458.
18. A. A. Nawaz, M. Urbanska, M. Herbig, M. Nötzel, M. Kräter, P. Rosendahl, C. Herold, N. Toepfner, M. Kubánková, R. Goswami, S. Abuhattum, F. Reichel, P. Müller, A. Taubenberger, S. Girardo, A. Jacobi and J. Guck, *Nat. Methods*, 2020, **17**, 595-599.
19. A. Lee, J. Park, M. Lim, V. Sunkara, S. Y. Kim, G. H. Kim, M.-H. Kim and Y.-K. Cho, *Anal. Chem.*, 2014, **86**, 11349-11356.
20. T. Gao, Z. Mao, W. Li and R. Pei, *J. Mater. Chem. B*, 2021, **9**, 746-756.
21. K. Bacon, A. Lavoie, B. M. Rao, M. Daniele and S. Menegatti, *Acta Biomater.*, 2020, **112**, 29-51.
22. F. Mohr, S. Przibilla, F. Leonhardt, C. Stemberger, S. Dreher, T. R. Mueller, S. P. Fraessle, G. P. Schmidt, M.-L. Kiene, H. Stadler and D. H. Busch, *Sci. Rep.*, 2018, **8**, 16731.
23. A. Srivastava, A. K. Shakya and A. Kumar, *Enzyme. Microb. Technol.*, 2012, **51**, 373-381.
24. G. Xu, Y. Tan, T. Xu, D. Yin, M. Wang, M. Shen, X. Chen, X. Shi and X. Zhu, *Biomater. Sci.*, 2017, **5**, 752-761.
25. R. Saranya, R. Murugan, M. Hegde, J. Doyle and R. Babu, *Affinity Membranes for Capture of Cells and Biological Substances*. Springer, Cham, Switzerland, 2018.
26. M. Gonzalez-Gonzalez and M. Rito-Palomares, *J. Mol. Recognit.*, 2015, **28**, 142-147.
27. M. Gonzalez-Gonzalez, R. C. Willson and M. Rito-Palomares, *Sep. Purif. Technol.*, 2016, **158**, 103-107.
28. L. Wu, Y. Wang, L. Zhu, Y. Liu, T. Wang, D. Liu, Y. Song and C. Yang, *Acs Appl. Bio Mater.*, 2020, **3**, 2743-2764.
29. J. Li, C. Qi, Z. Lian, Q. Han, X. Wang, S. Cai, R. Yang and C. Wang, *Acs Appl. Mater. Interfaces*, 2016, **8**, 2511-2516.
30. H. Shen, J. Yang, Z. Chen, X. Chen, L. Wang, J. Hu, F. Ji, G. Xie and W. Feng, *Biosens. Bioelectron.*, 2016, **81**, 495-502.
31. N. Sun, M. Liu, J. Wang, Z. Wang, X. Li, B. Jiang and R. Pei, *Small*, 2016, **12**, 5090-5097.
32. Y. Lin, L. Jiang, Y. Huang, Y. Yang, Y. He, C. Lu and H. Yang, *Chem. Commun.*, 2019, **55**, 5387-5390.
33. T.-T. Zhai, D. Ye, Q.-W. Zhang, Z.-Q. Wu and X.-H. Xia, *Acs Appl. Mater. Interfaces*, 2017, **9**, 34706-34714.
34. K. A. Hyun, T. Y. Lee, S. H. Lee and H. I. Jung, *Biosens. Bioelectron.*, 2015, **67**, 86-92.
35. S. Sun, S. Yang, X. Hu, C. Zheng, H. Song, L. Wang, Z. Shen and Z. S. Wu, *ACS Sens.*, 2020, **5**, 3870-3878.
36. A. C. Fisher, M. H. Kamga, C. Agarabi, K. Brorson, S. L. Lee and S. Yoon, *Trends Biotechnol.*, 2019, **37**, 253-267.
37. P. H. Chen, Y. T. Cheng, B. S. Ni and J. H. Huang, *Appl. Biochem. Biotechnol.*, 2020, **191**, 151-163.
38. X. Gong, C. Hou, Q. Zhang, Y. Li and H. Wang, *ACS Appl. Mater. Interfaces*, 2020, **12**, 51225-51235.
39. M. Qu, X. Jiang, X. Zhou, C. Wang, Q. Wu, L. Ren, J. Zhu, S. Zhu, P. Tebon, W. Sun and A. Khademhosseini, *Adv. Healthcare Mater.*, 2020, **9**, 1901714.
40. A. Shastri, L. M. McGregor, Y. Liu, V. Harris, H. Nan, M. Mujica, Y. Vasquez, A. Bhattacharya, Y. Ma, M. Aizenberg, O. Kuksenok, A. C. Balazs, J. Aizenberg and X. He, *Nat. Chem.*, 2015, **7**, 447-454.
41. J. M. Klco and C. G. Mullighan, *Nat. Rev. Cancer.*, 2021, **21**, 122-137.
42. K. A. Foon and R. F. Todd, *Blood*, 1986, **68**, 1-31.
43. X. Pang, C. Cui, M. Su, Y. Wang, Q. Wei and W. Tan, *Nano energy*, 2018, **46**, 101-109.
44. W. Niu, X. Chen, W. Tan and A. S. Veige, *Angew. Chem. Int. Ed. Engl.*, 2016, **55**, 8889-8893.

45. L. Ding, Y. Wu, Y. Duan, S. Yu, F. Yu, J. Wang, Y. Tian, Z. Gao, Z. Wan and L. He, *ACS Sens.*, 2020, **5**, 440-446.
46. Z. Chen, J. Liu, Y. Chen, X. Zheng, H. Liu and H. Li, *ACS Appl. Mater. Interfaces*, 2021, **13**, 1353-1366.
47. L. Yang, X. Fan, J. Zhang and J. Ju, *Polymers*, 2020, **12**, 389.
48. T. Sarwan, P. Kumar, Y. E. Choonara and V. Pillay, *Front. Mater.*, 2020, **7**, 73.
49. K. Nagase and T. Okano, *J. Mater. Chem. B*, 2016, **4**, 6381-6397.
50. Q. Zhang, W. Wang, S. Huang, S. Yu, T. Tan, J.R. Zhang and J.J. Zhu, *Chem. Sci.*, 2020, **11**, 1948-1956.
51. M. Abadier, A. B. Pramod, S. McArdle, A. Marki, Z. Fan, E. Gutierrez, A. Groisman and K. Ley, *Cell Rep.*, 2017, **21**, 3885-3899.
52. S. Okhota, I. Melnikov, Y. Avtaeva, S. Kozlov and Z. Gabbasov, *Int. J. Mol. Sci.*, 2020, **21**, 7804.
53. Y. Liu, O. Kuksenok, X. He, M. Aizenberg, J. Aizenberg and A. C. Balazs, *Acs Appl. Mater. Interfaces*, 2016, **8**, 30475-30483.
54. Y. Wang, N. Gan, Y. Zhou, T. Li, Y. Cao and Y. Chen, *Biosens. Bioelectron.*, 2017, **87**, 508-513.
55. J. A. Reed, A. E. Lucero, M. A. Cooperstein and H. E. Canavan, *J. Appl. Biomater. Biomech.*, 2008, **6**, 81-88.
56. J. Tan, Z. Lai, L. Zhong, Z. Zhang, R. Zheng, J. Su, Y. Huang, P. Huang, H. Song, N. Yang, S. Zhou and Y. Zhao, *Nanoscale Res. Lett.*, 2018, **13**, 66.
57. X. Pang, C. Cui, M. Su, Y. Wang, Q. Wei and W. Tan, *Nano energy*, 2018, **46**, 101-109.
58. W. Liang, J. Liu, X. Yang, Q. Zhang, W. Yang, H. Zhang and L. Liu, *Microfluid. Nanofluid.*, 2020, **24**, 26.
59. S. Zhu, D. Wu, Y. Han, C. Wang, N. Xiang and Z. Ni, *Lab Chip*, 2020, **20**, 244-252.
60. J. F. Edd, A. Mishra, T. D. Dubash, S. Herrera, R. Mohammad, E. K. Williams, X. Hong, B. R. Mutlu, J. R. Walsh, F. M. de Carvalho, B. Aldikacti, L. T. Nieman, S. L. Stott, R. Kapur, S. Maheswaran, D. A. Haber and M. Toner, *Lab Chip*, 2020, **20**, 558-567.
61. S. Dey, R. Vaidyanathan, L. G. Carrascosa, M. J. A. Shiddiky and M. Trau, *Acs Sens.*, 2016, **1**, 399-405.
62. S. Dey, K. M. Koo, Z. Wang, A. A. I. Sina, A. Wuethrich and M. Trau, *Lab Chip*, 2019, **19**, 738-748.
63. Y. Zhou and R. M. Raphael, *Biophys. J.*, 2007, **92**, 2451-2462.
64. K. K. Dijkstra, C. M. Cattaneo, F. Weeber, M. Chalabi, J. van de Haar, L. F. Fanchi, M. Slagter, D. L. van der Velden, S. Kaing, S. Kelderman, N. van Rooij, M. E. van Leerdam, A. Depla, E. F. Smit, K. J. Hartemink, R. de Groot, M. C. Wolkers, N. Sachs, P. Snaebjornsson, K. Monkhorst, J. Haanen, H. Clevers, T. N. Schumacher and E. E. Voest, *Cell*, 2018, **174**, 1586-1598.e1512.
65. D. Shangguan, Y. Li, Z. Tang, Z. C. Cao, H. W. Chen, P. Mallikaratchy, K. Sefah, C. J. Yang and W. Tan, *Proc. Natl. Acad. Sci. U. S. A.*, 2006, **103**, 11838.
66. J. Zhou and J. Rossi, *Nat. Rev. Drug Discovery*, 2017, **16**, 181-202.
67. Z. Zhang, N. Chen, S. Li, M. R. Battig and Y. Wang, *J. Am. Chem. Soc.*, 2012, **134**, 15716-15719.



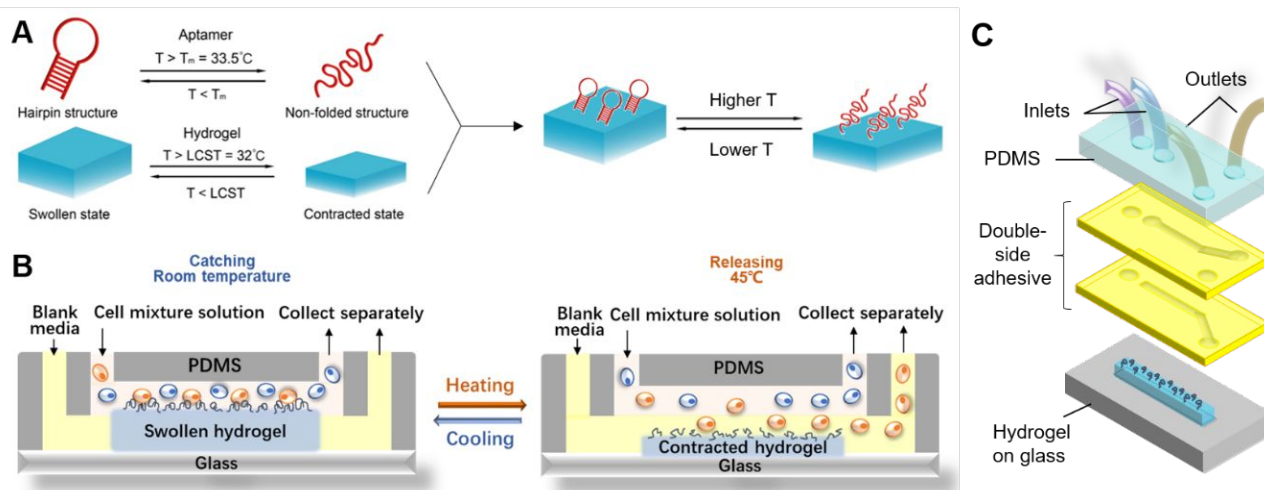


**Fig. 1** **A.** The reversible response to temperature of aptamer, hydrogel and aptamer-functionalized hydrogel. **B.** The cell separation mechanism of the iCatch microfluidic device consisting an aptamer-functionalized hydrogel placed in microfluidic channels. **C.** The design of the iCatch consisting an aptamer-functionalized hydrogel placed in microfluidic channels with two inlets respectively leading to the upper and lower streams and two outlets.



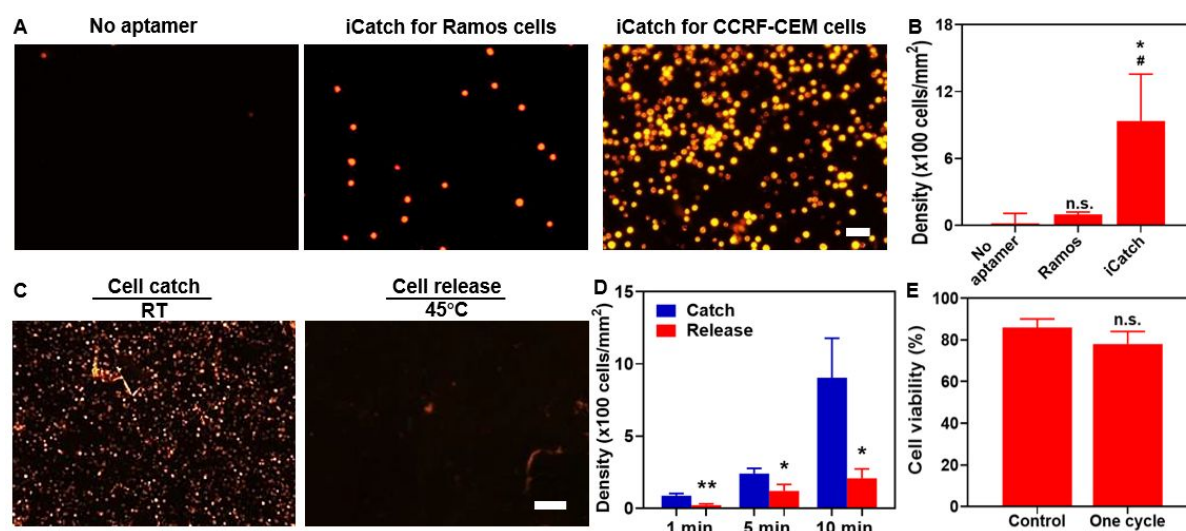


**Fig. 3 A.** Confocal microscopic images of cell captured on the PNIPAAm hydrogel. Left image: bare PNIPAAm hydrogel without aptamer decoration. Middle and right images: sgc8c aptamer decorated hydrogel for Ramos cell (middle) and CCRF-CEM cell (right) capture. (scale bar = 50  $\mu\text{m}$ ) **B.** Quantification of Ramos and CCRF-CEM cell attachment on PNIPAAm hydrogel without or with aptamer decoration, respectively. Unpaired t test was performed for analysis. \* $p < 0.05$ , compared with the group without aptamers. # $p < 0.05$ , compared with the group with Ramos cells. **C.** Microscopic images of CCRF-CEM cell remaining on the hydrogel after 10 min cell capture at RT and cell releasing at 45°C. (scale bar = 200  $\mu\text{m}$ ) **D.** Analysis of cell density on the hydrogel after incubating cells with iCatch for 1, 5, and 10 min and releasing subsequently. Unpaired t test was performed for analysis. \* $p < 0.05$ , \*\* $p < 0.05$ . **E.** Quantifications of cell viability after one catch-and-release cycle by performing Live/Dead staining assay. Unpaired t test was performed. n.s., no significant statistical difference. All experiments were performed in triplicate.

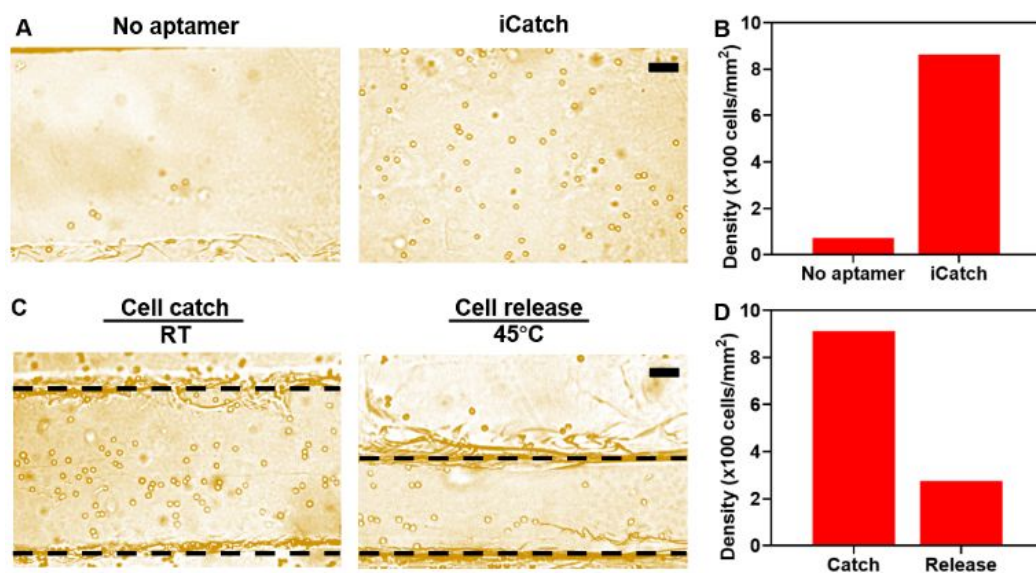


**Fig. 4** **A.** Bright field microscopic images of CCRF-CEM cell capture in the iCatch microfluidic device without (left) and with (right) aptamers. **B.** Quantification of CCRF-CEM cells on the device with or without aptamers. **C.** top-view optical images of cell catch-and-release process. The dashed lines demarcate the location of hydrogel. Left image: when the temperature is at RT, cells are captured, and hydrogel is swelling; Right image: when the temperature is increased to 45°C, cells are released due to the denature of aptamers and hydrogel contracts to generation movement for cell transportation. **D.** Cell catch and release on iCatch quantification. All scale bars are 50  $\mu$ m.